Electronic Supplementary Material (ESI) for RSC Advances.

Supporting Information

Fabrication of a new metal-organic framework for sensitive sensing of nitroaromatics and efficient dye adsorption

Wei-Ping Wu[a*], Jian Wu[b], Jian-Qiang Liu[c*], Manoj Trivedi[d] and Abhinav Kumar[d*]

Sensing Method

The photoluminescence sensing were performed as follows: the photoluminescence properties of **1** were investigated in N,N-dimethylformamide (DMF)/H_2O emulsions at room temperature using a RF-5301PC spectrofluorophotometer. The **1**@DMF/H_2O elusions were prepared by adding 5 mg of **1** powder into 3.00 mL of DMF and then ultrasonic agitation the mixture for 30 min before testing.

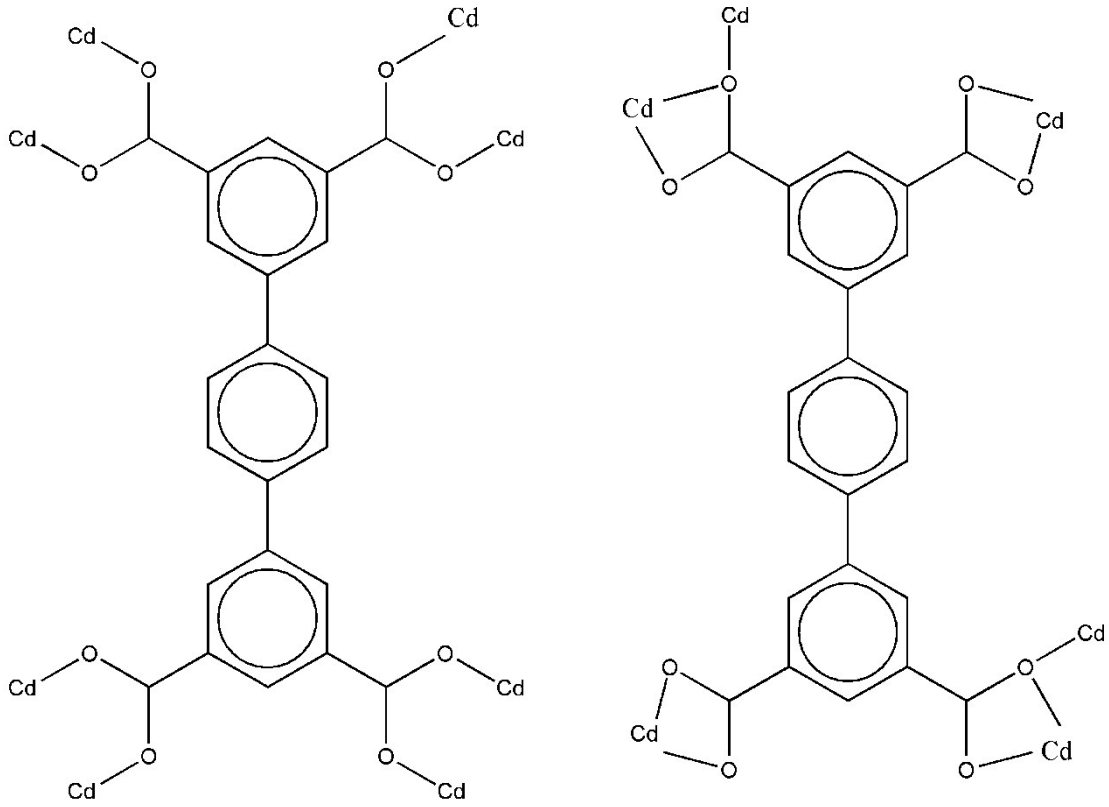

Scheme S1 view of the two coordination modes of H_4L ligand in this work.

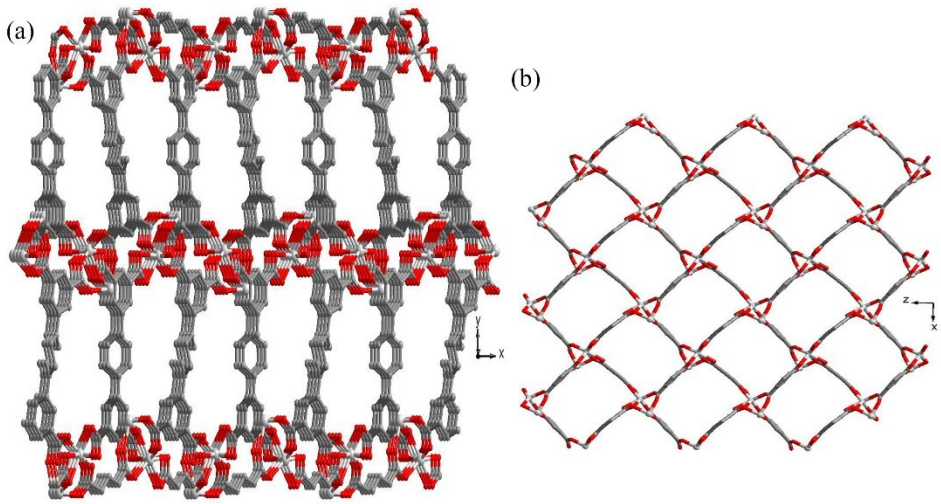

Fig. S1 view of the 3D network along the *ab*-plane.

Based upon the single crystal structure analysis, **1** has nano-sized pores. To reveal the thermal stability of these porous compounds, thermo-gravimetric experiments were carried out with pure single crystal samples under N_2 atmosphere conditions at a rate of 10 °C min^{-1} over a range of 25–800 °C. In Fig. S2, the TGA curve of **1** shows two regions of weight loss. The first weight loss between 100 and 350 °C is about 28.6 %, which corresponds to the loss of three coordinated and a half free DMF molecules, calculated to be28.1%. Above 350 °C, the compound decomposed gradually.

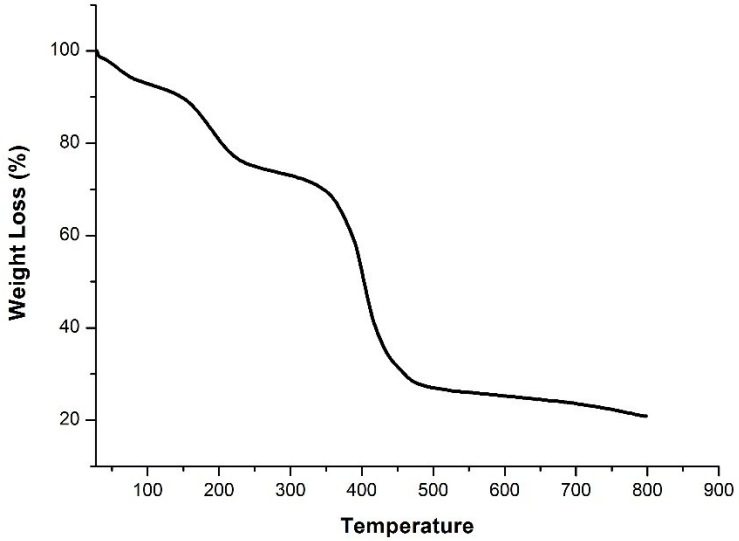

Fig. S2 view of TGA in **1**.

Gas Sorption

The nitrogen adsorption-desorption measurements were carried out at liquid nitrogen temperature (77 K) by using an automatic volumetric adsorption equipment (Micromeritics, ASAP2020). Low pressure (< 800 torr) gas sorption isotherms were performed using a Micromeritics ASAP 2020 surface area and pore size analyzer. Pore size distribution data were obtained from the N_2 sorption isotherms based on the DFT model in the Micromeritics ASAP 2020 software package (assuming slit pore geometry). An ultra-high purity (UHP, 99.999% purity) grade of N_2 gas was used throughout the adsorption experiments. Prior to the measurements, all the samples were degassed at 80 ºC for 10 h to remove the adsorbed impurities.

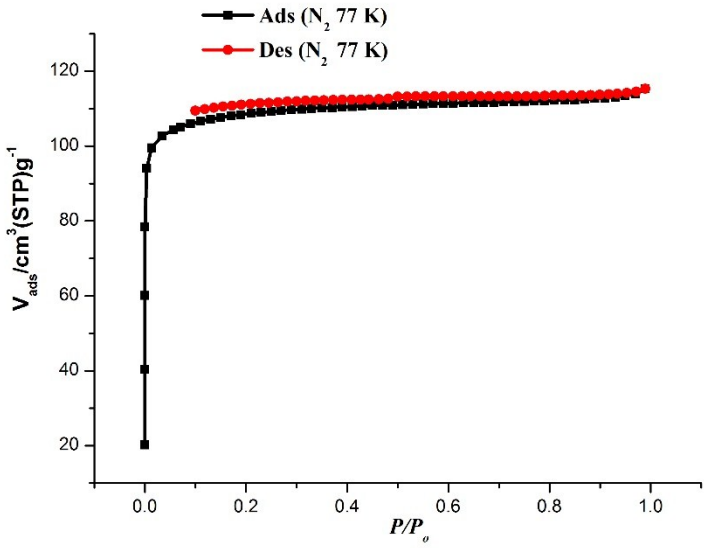

Fig. S3 view of the N_2 adsorption isotherms at 77 K.

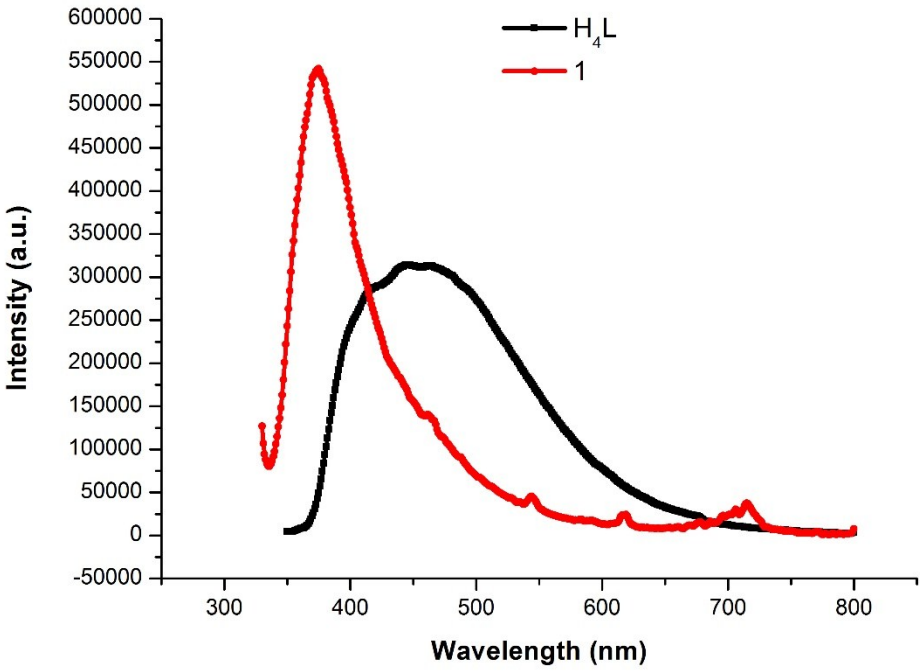

Fig. S4 view of the PL for solid state of **1** and H_4L at room temperature.

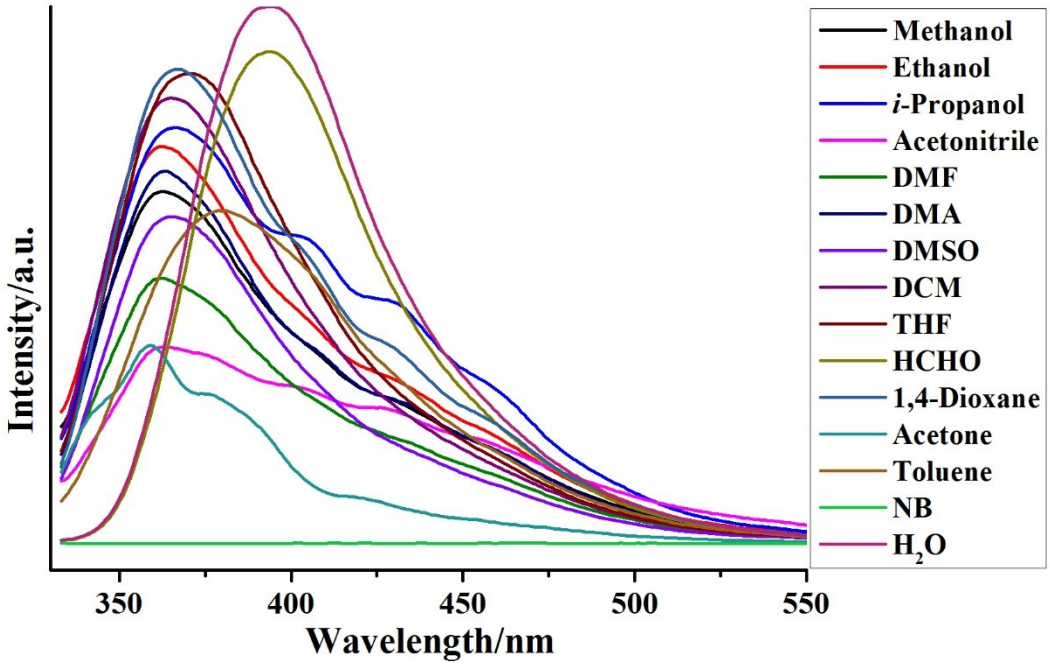

Fig. S5 Emission spectra of **1** at different solvents.

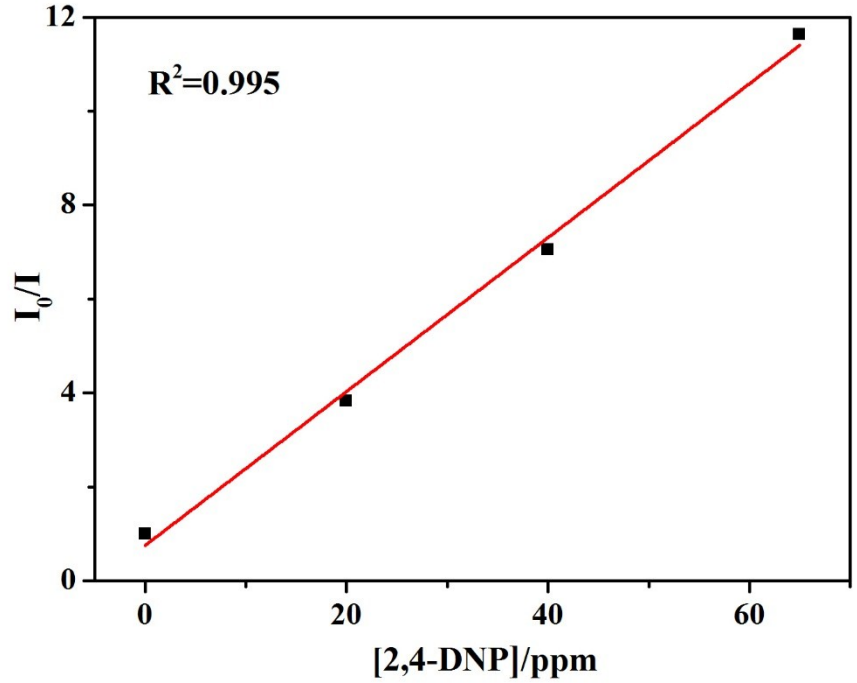

Fig. S6 Stern–Volmer plot for the fluorescence quenching of **1** upon the addition of 2,4-DNP.

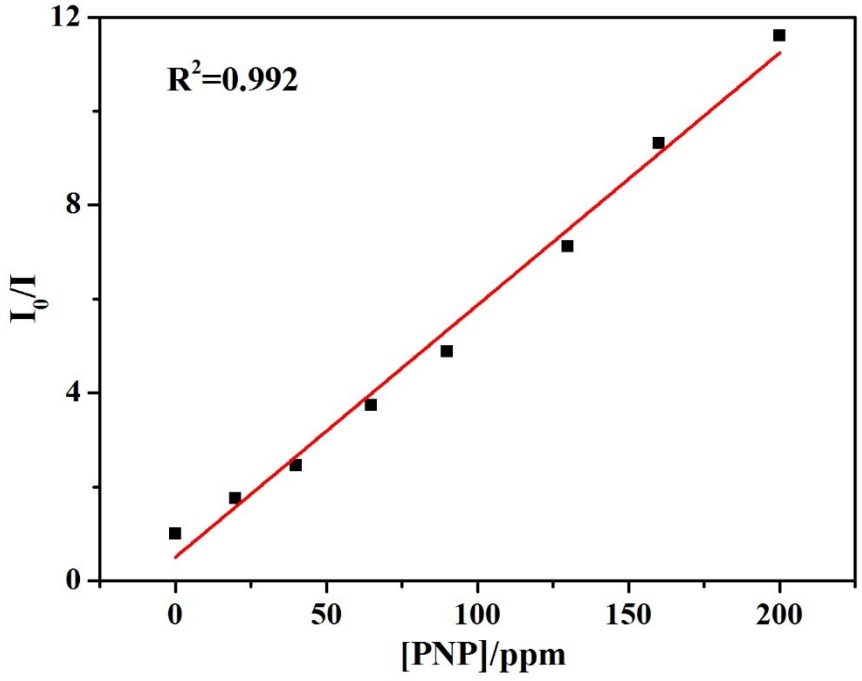

Fig. S7 Stern–Volmer plot for the fluorescence quenching of **1** upon the addition of PNP.

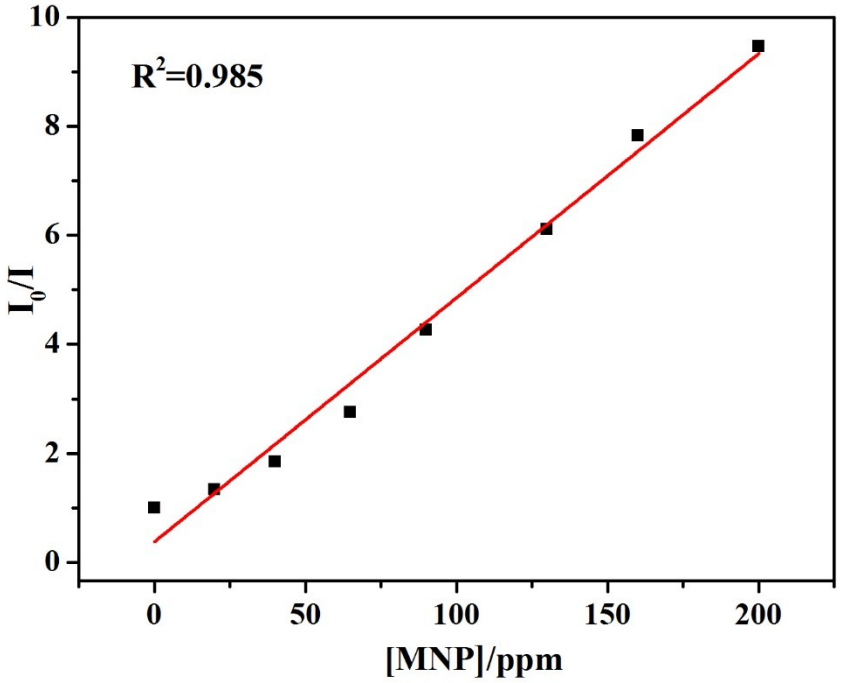

Fig. S8 Stern–Volmer plot for the fluorescence quenching of **1** upon the addition of MNP.

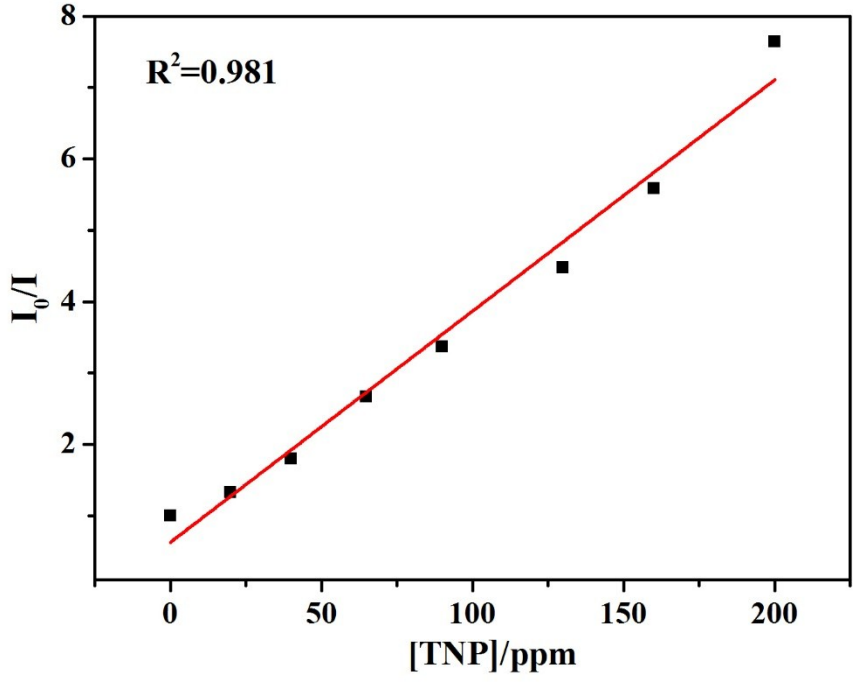

Fig. S9 Stern–Volmer plot for the fluorescence quenching of **1** upon the addition of TNP.

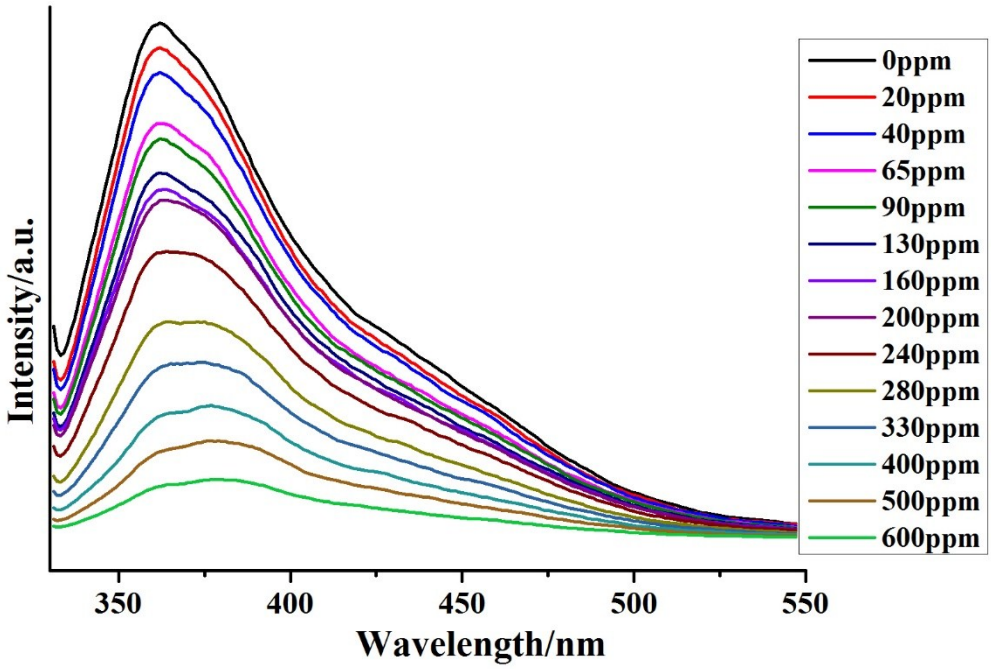

Fig. S10 Luminescent quenching of **1** dispersed in ethanol by the gradual addition of 1 mM solution of 1,3-DNB in DMF.

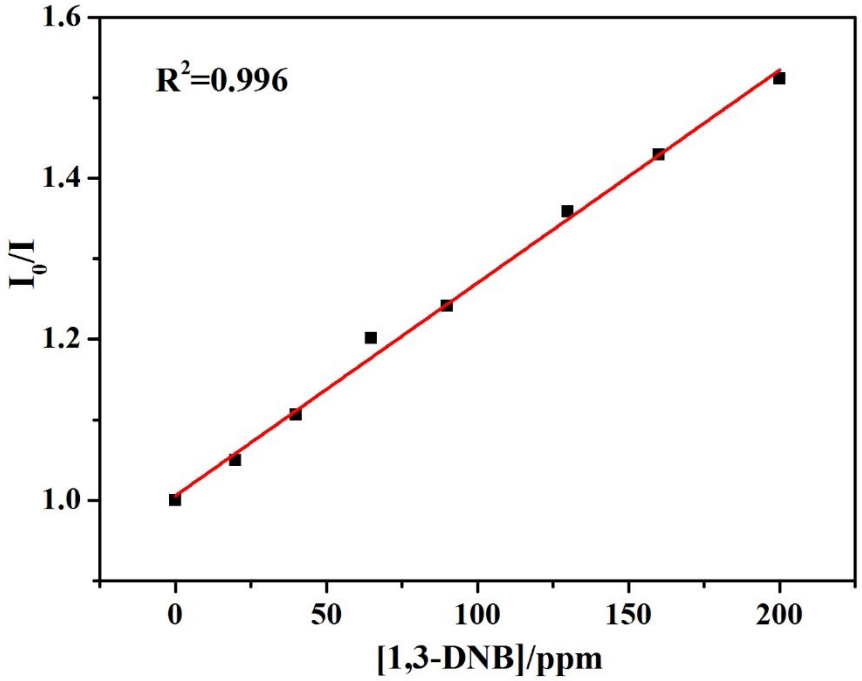

Fig. S11 Stern–Volmer plot for the fluorescence quenching of **1** upon the addition of 1,3-DNB.

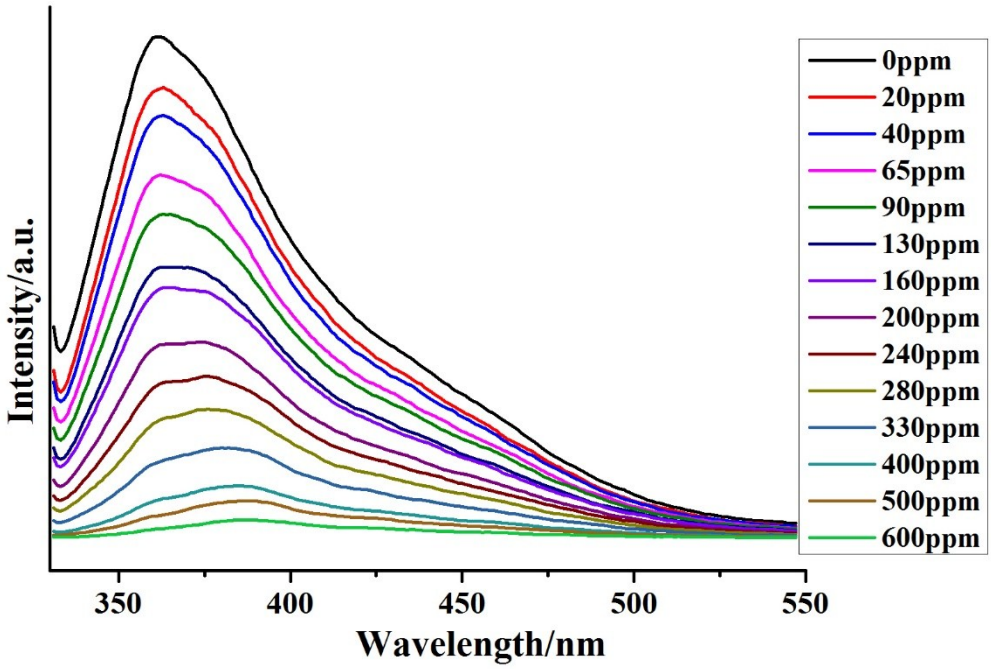

Fig. S12 Luminescent quenching of **1** dispersed in ethanol by the gradual addition of 1 mM solution of 2,4-DNT in DMF.

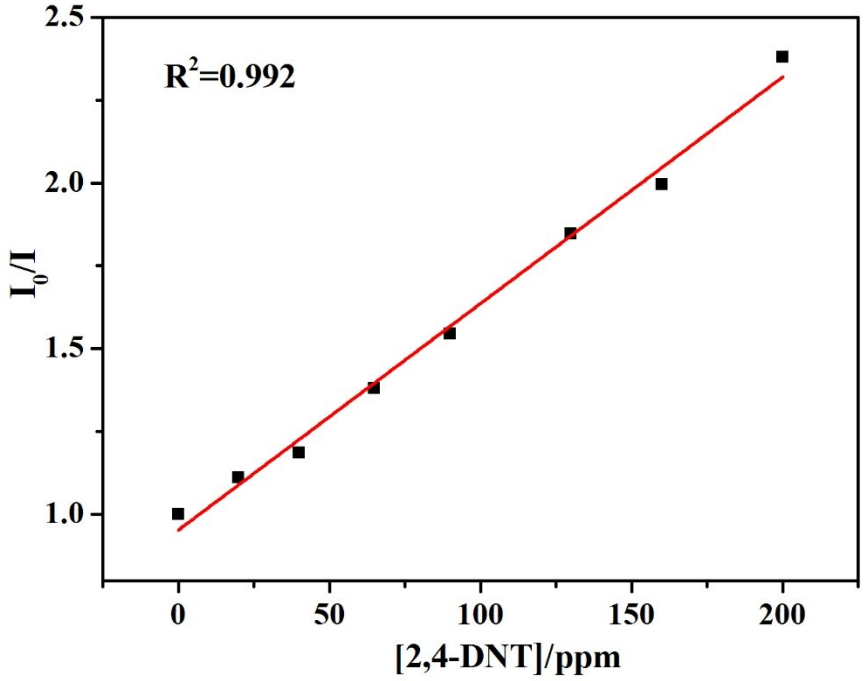

Fig. S13 Stern–Volmer plot for the fluorescence quenching of **1** upon the addition of 2,4-DNT.

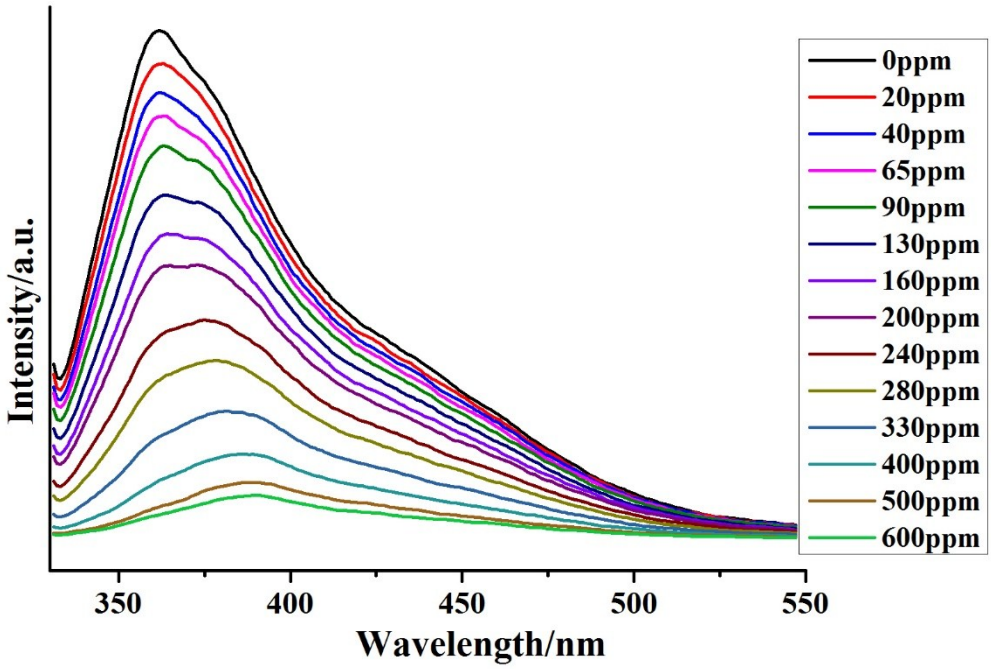

Fig. S14 Luminescent quenching of **1** dispersed in ethanol by the gradual addition of 1 mM solution of 2,6-DNT in DMF.

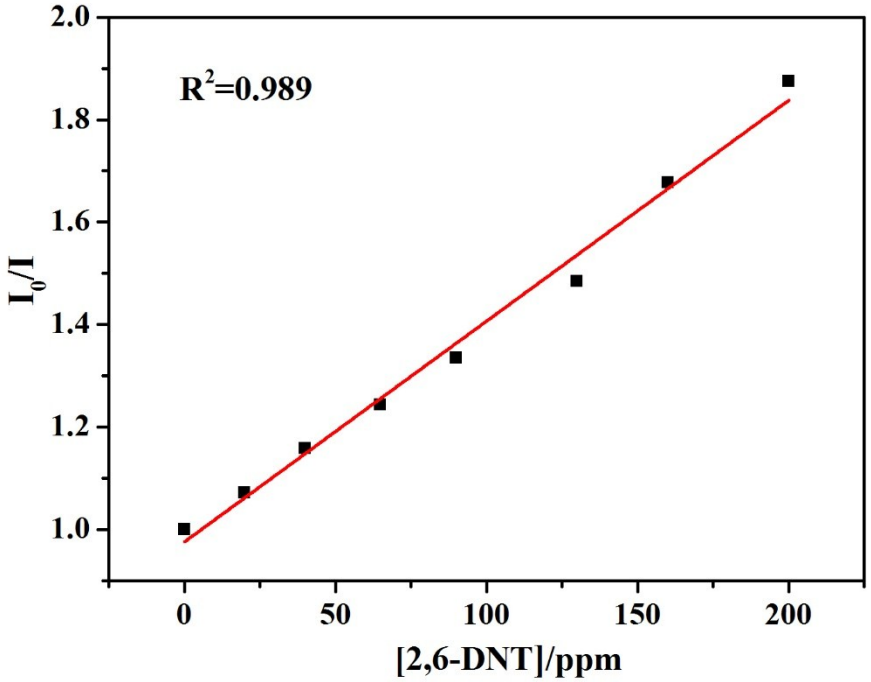

Fig. S15 Stern–Volmer plot for the fluorescence quenching of **1** upon the addition of 2,6-DNT.

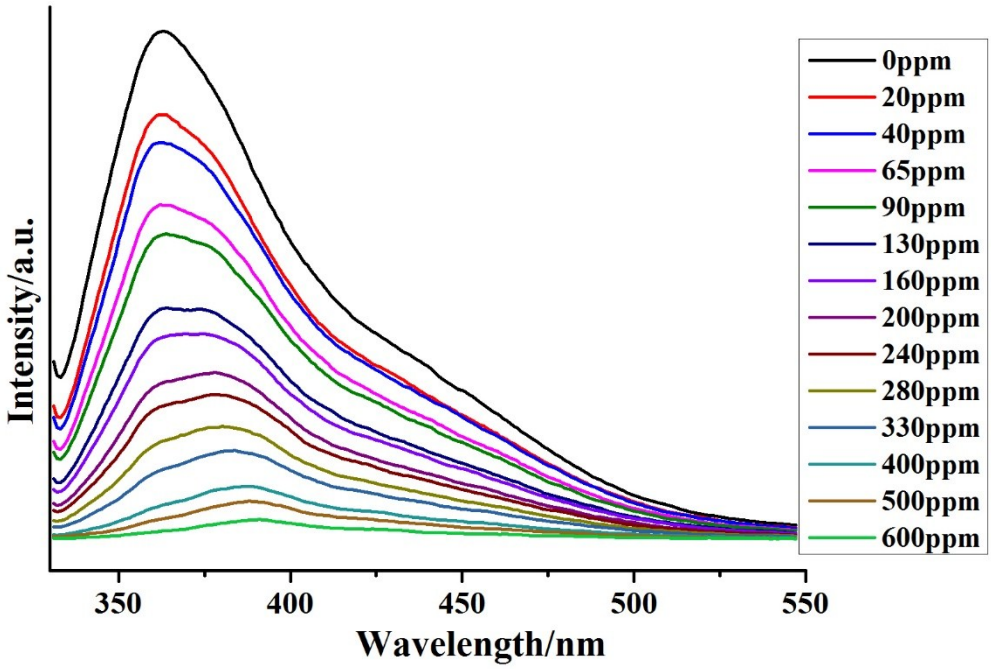

Fig. S16 Luminescent quenching of **1** dispersed in ethanol by the gradual addition of 1 mM solution of 2-NT in DMF.

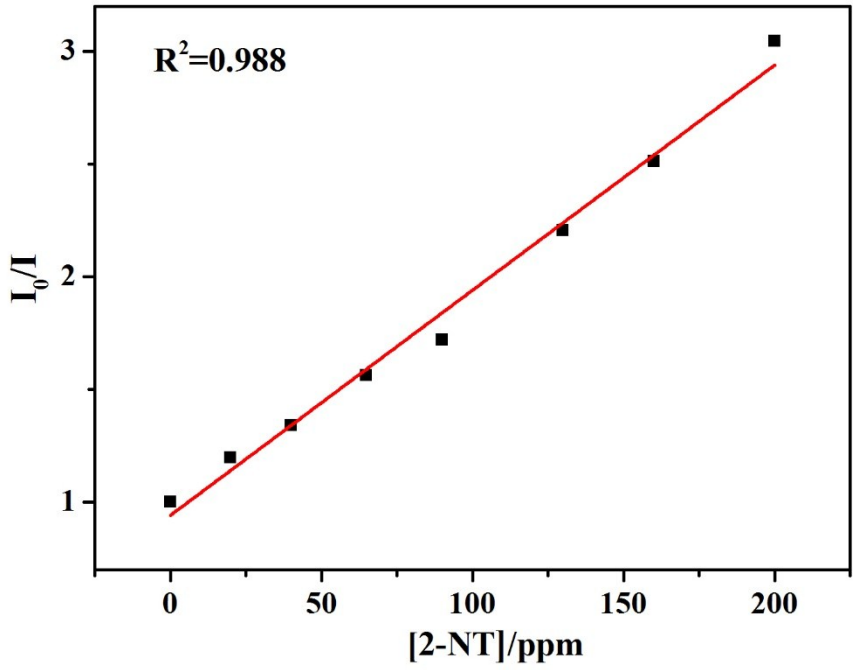

Fig. S17 Stern–Volmer plot for the fluorescence quenching of **1** upon the addition of 2-NT.

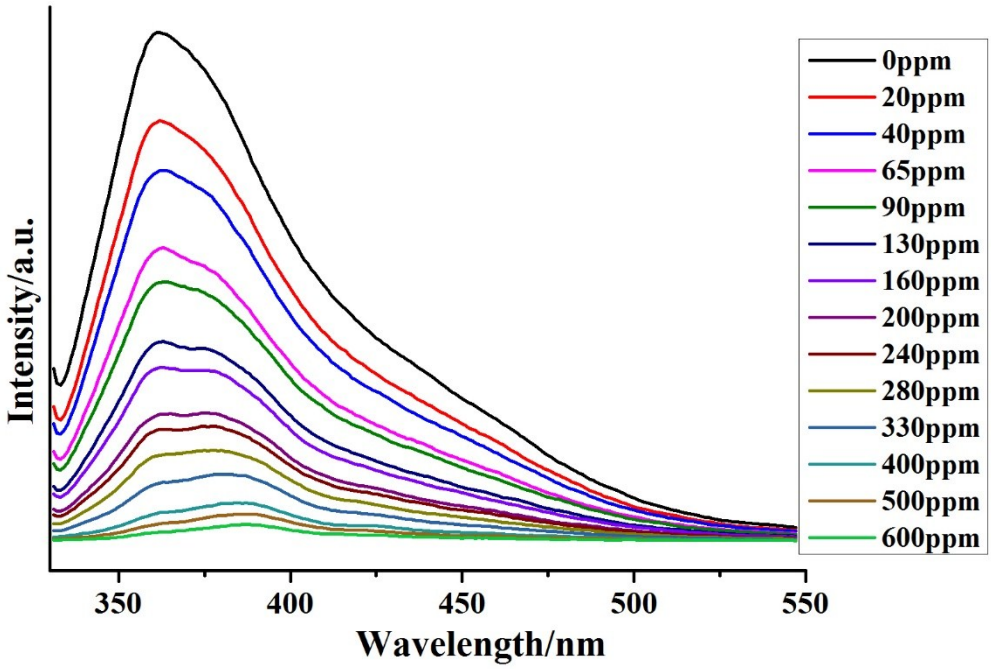

Fig. S18 Luminescent quenching of **1** dispersed in ethanol by the gradual addition of 1 mM solution of 4-NT in DMF.

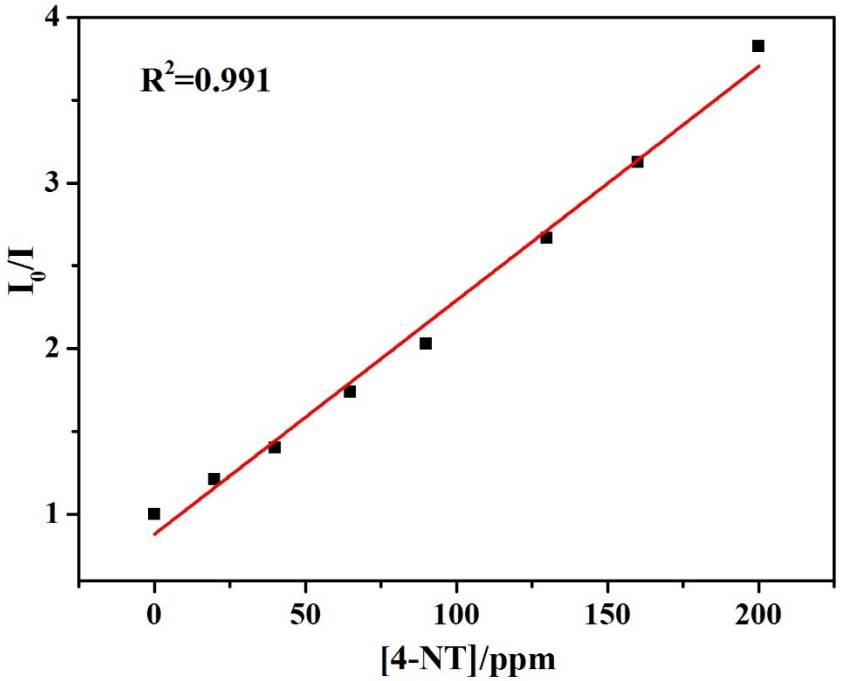

Fig. S19 Stern–Volmer plot for the fluorescence quenching of **1** upon the addition of 4-NT.

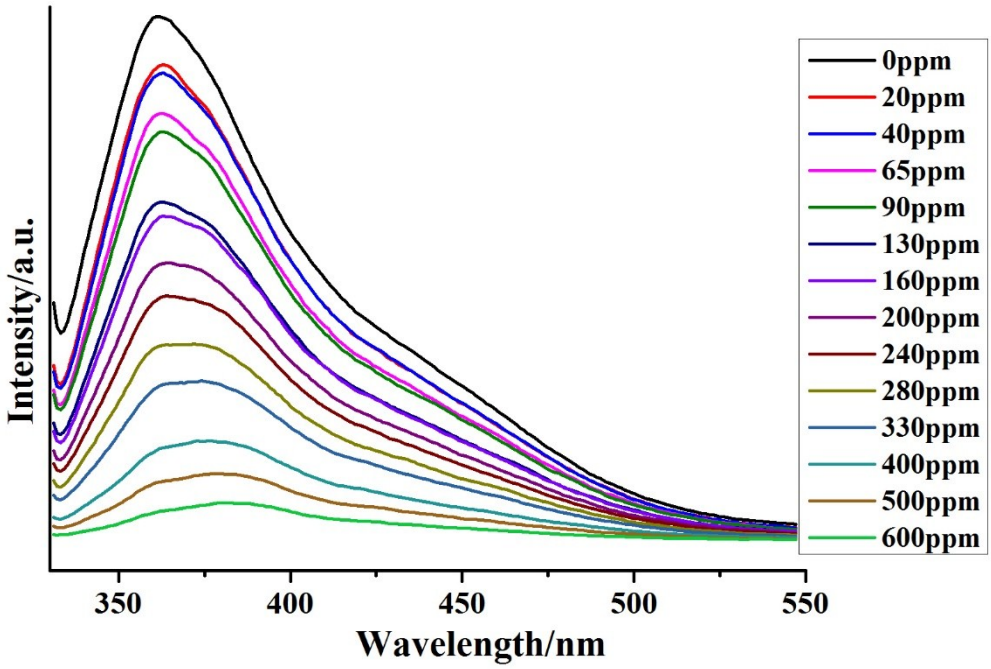

Fig. S20 Luminescent quenching of **1** dispersed in ethanol by the gradual addition of 1 mM solution of NB in DMF.

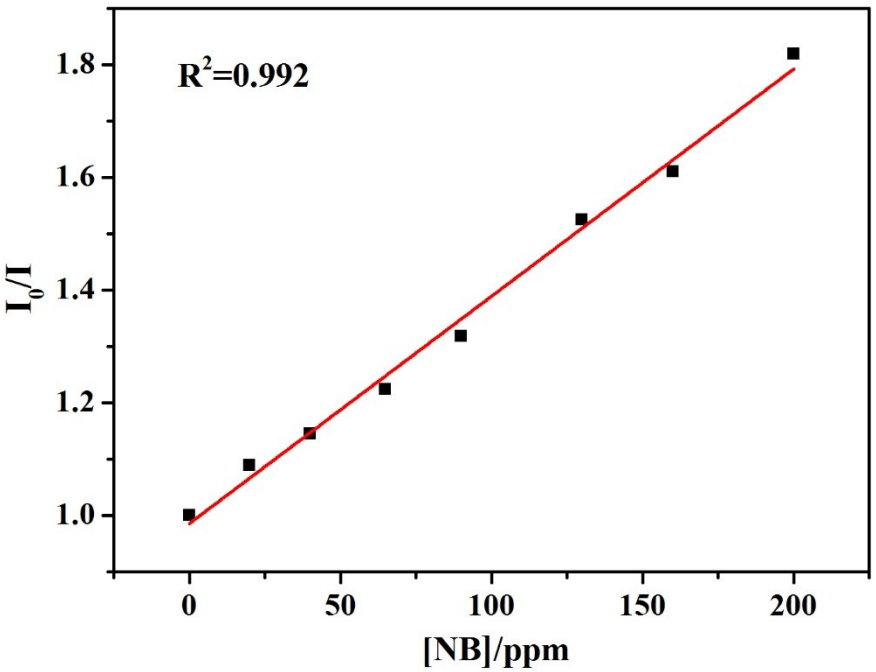

Fig. S21 Stern–Volmer plot for the fluorescence quenching of **1** upon the addition of NB.

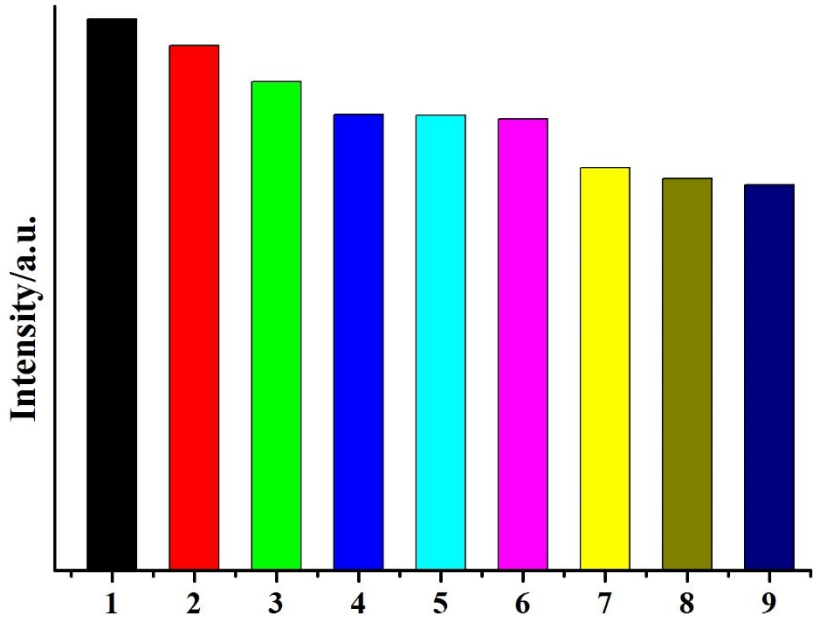

Fig. S22 Luminescent quenching of H_4L dispersed in ethanol by the gradual addition of 1 mM solution of 2,4-DNP in DMF.

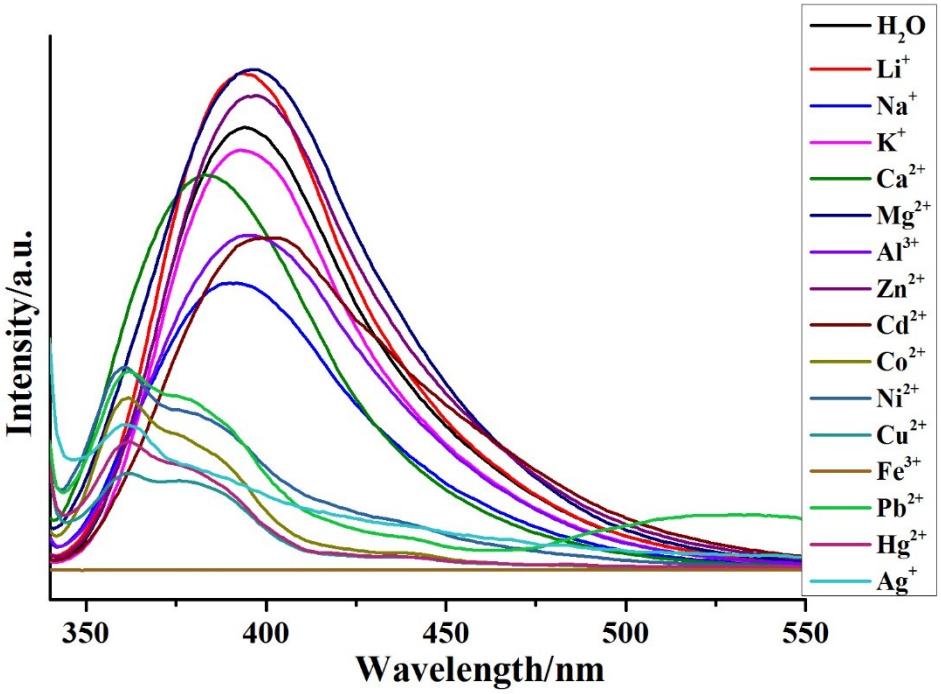

Fig. S23 Emission spectra of **1** at different metal ions.

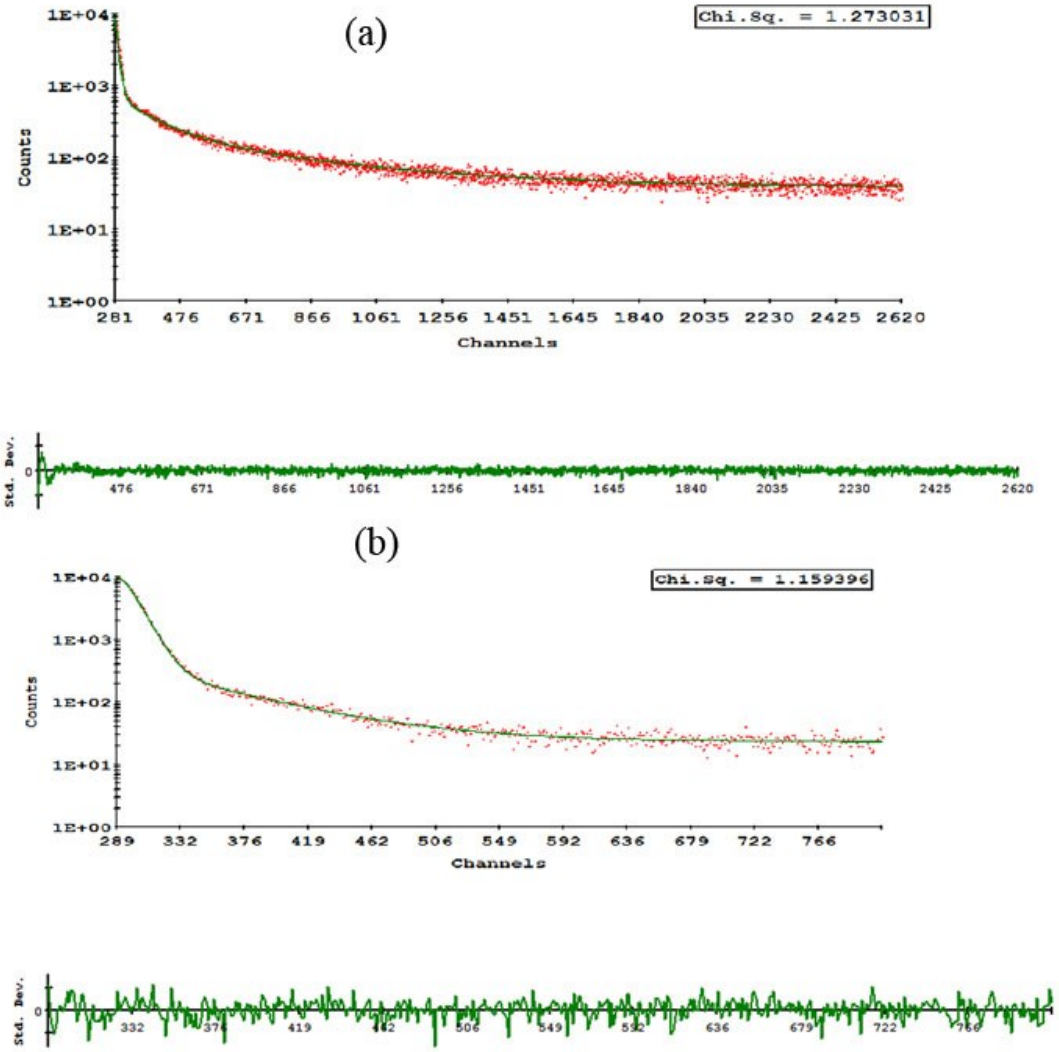

Fig. S24 Comparison of the fluorescence lifetime studies of original samples (a) and Fe^{3+}-infused **1** in 10^{-2} $Fe(NO_3)_3$ DMF solution (b).

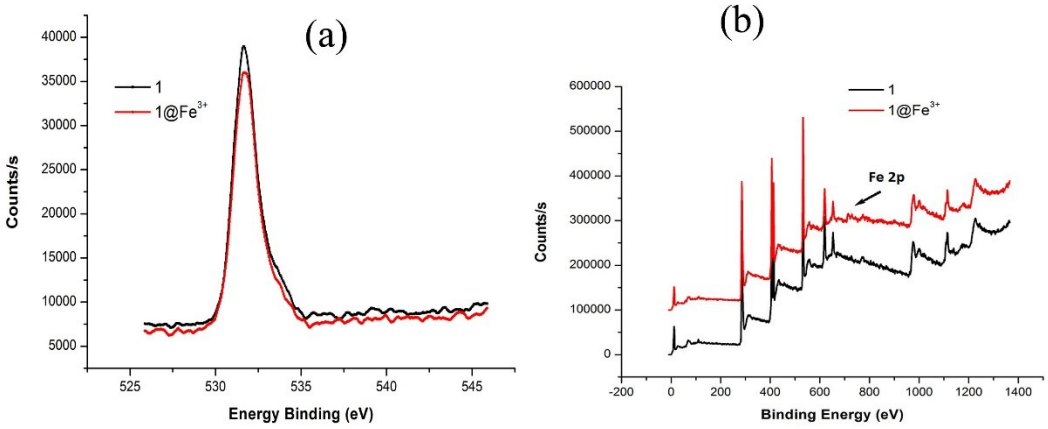

Fig. S25. (a) O1s XPS spectra of the original **1** (black) and **1**@Fe^{3+} (red); (b) XPS spectra of the **1**@Fe^{3+} (red) and original **1** (black).

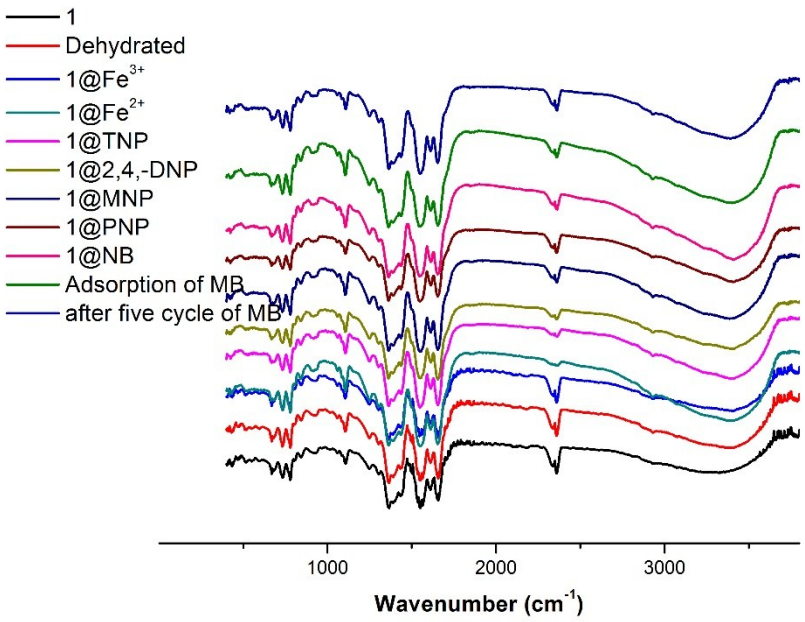

Fig. S26 view of the IR in different inclusions.

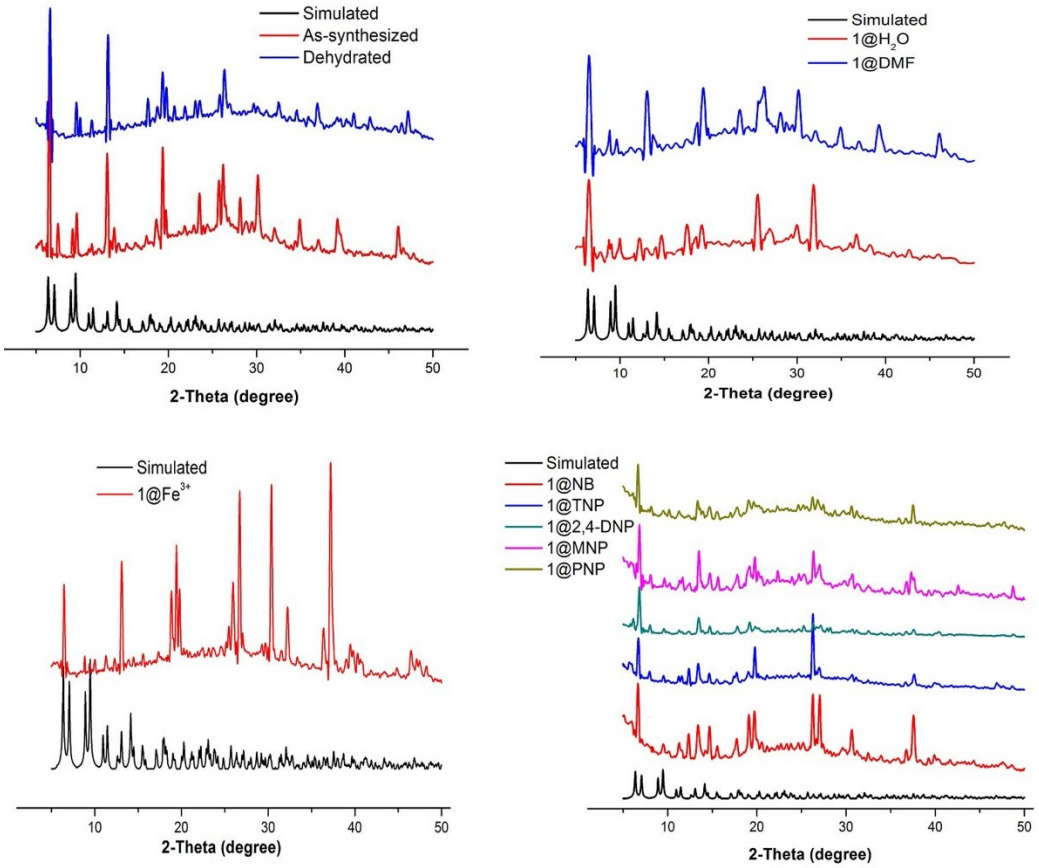

Fig. S27 (a) view of the PXRD for the sample **1** (black: simulated; red: as-synthesized; blue: dehydrated ones); (b) view of the PXRD pattern of **1** at DMF and H_2O suspension; (c) view of the PXRD pattern of **1** at Fe^{3+} suspension; (c) view of the PXRD pattern of **1** dispersed in different explosives.

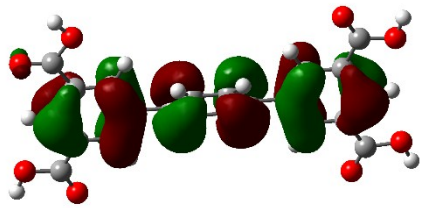 HOMO H_5L	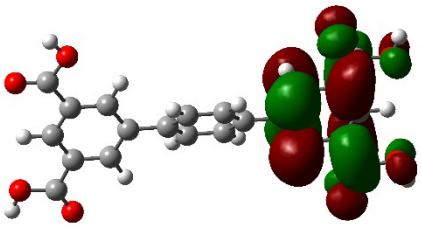 LUMO H_5L
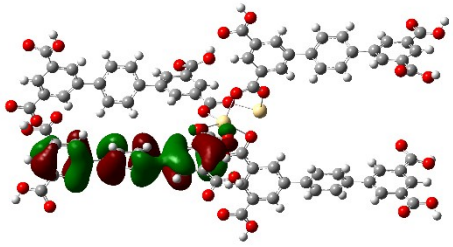 HOMO **1**	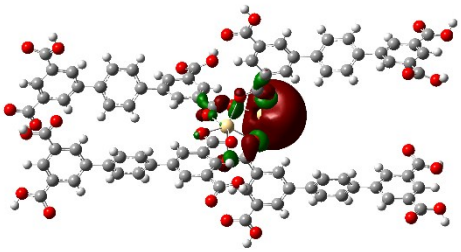 LUMO **1**
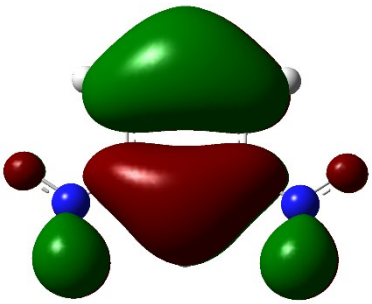 HOMO 1,3-DNB	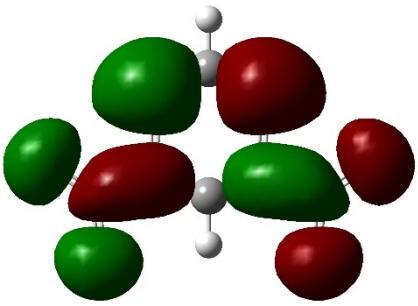 LUMO 1,3-DNB
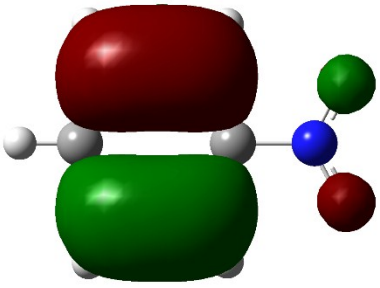 HOMO NB	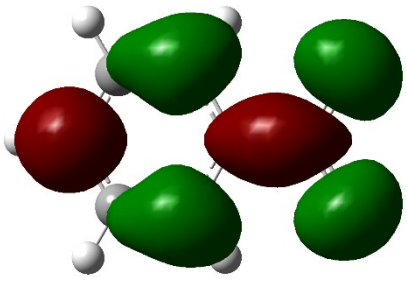 LUMO NB
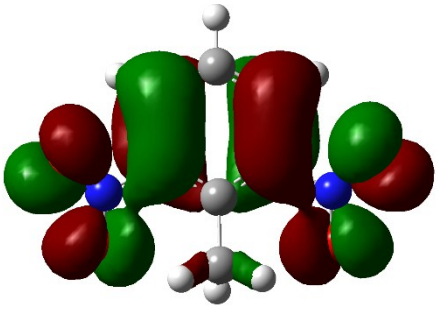 HOMO 2,6-DNT	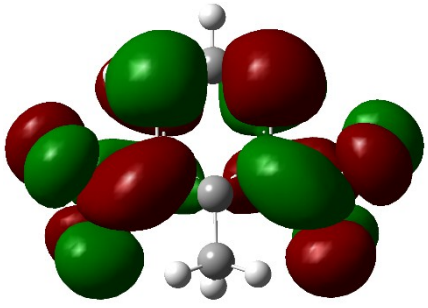 LUMO 2,6-DNT

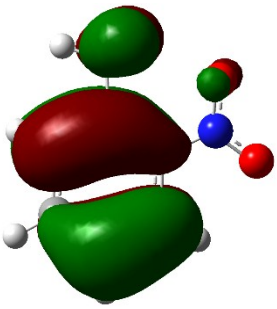 HOMO 2-NT	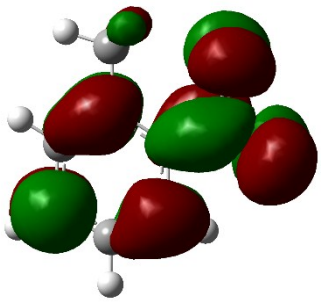 LUMO 2-NT
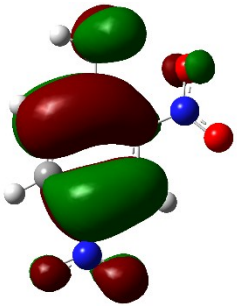 HOMO 2,4-DNT	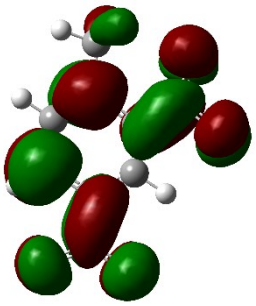 LUMO 2,4-DNT
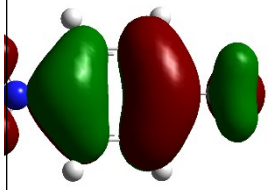 HOMO 4-NT	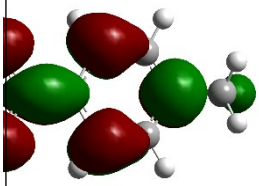 LUMO 4-NT
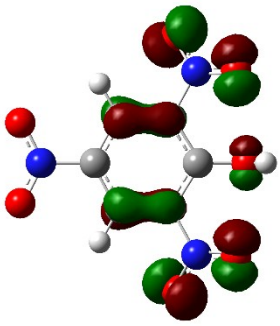 HOMO TNP	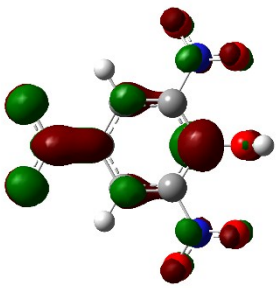 LUMO TNP

Fig. S28 HOMO-LUMO plots of H_4L, **1** and NACs

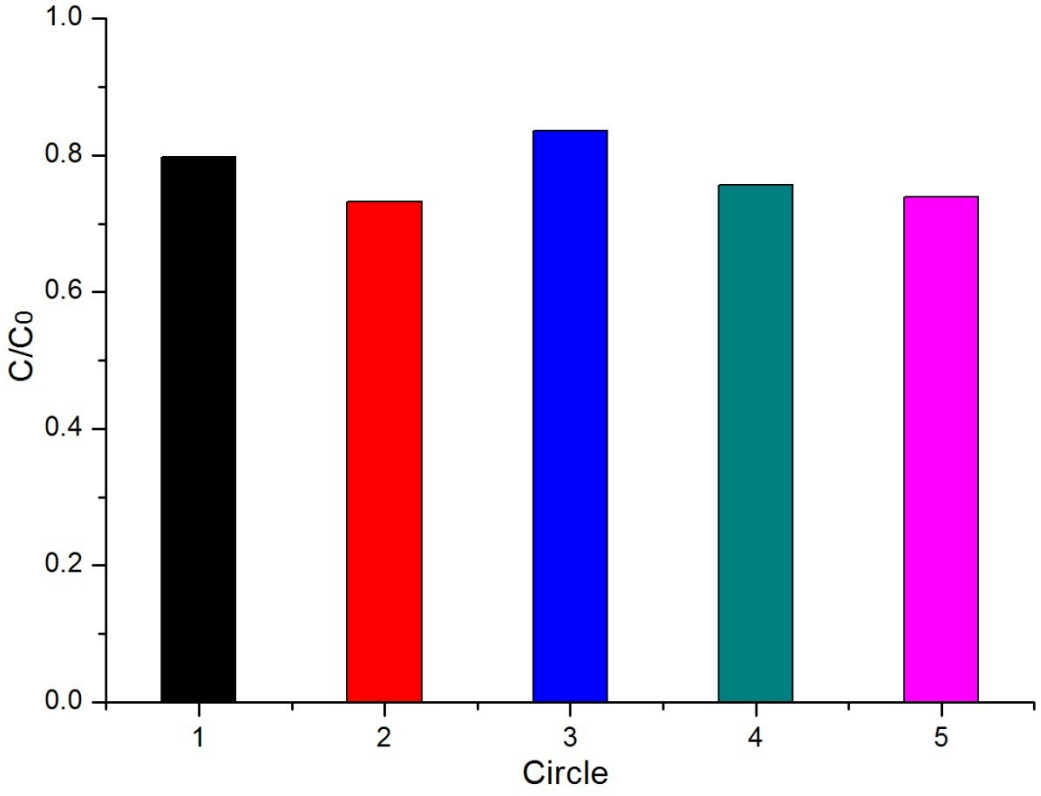

Fig. S29 view the cycle adsorption for the MB in **1.**

Table S1. Crystallographic data and structure refinement details for 1

Crystal system	Orthorhombic
Space group	$P2_12_12_1$
Crystal color	colorless
a, Å	14.0179(19)
b, Å	27.727(4)
c, Å	14.0053(19)
α, °	90
β, °	90
γ, °	90
V, Å ^{3}	5443.6(13)
Z	2
ρ_{calcd}, g/cm^3	1.033
μ, mm^{-1}	0.819
F(000)	1688

θ Range, deg	2.10-25.40
Reflection collected	60770
Independent reflections (R_{int})	0.0747
Reflections with $I > 2\sigma(I)$	17117
Number of parameters	530
R_1, wR_2 ($I > 2\sigma(I)$)*	0.0786, 0.1879
R_1, wR_2 (all data)**	0.1278, 0.2157

* $R = \sum(F_o - F_c)/\sum(F_o)$, ** $wR_2 = \{\sum[w(F_o^2 - F_c^2)^2]/\sum(F_o^2)^2\}^{1/2}$.

Table S2. Selected bond distances (Å) and angles (deg) for **1**

		1	
Cd(1)-O(5)	2.198(10)	Cd(1)-O(7)	2.208(10)
Cd(1)-O(4)	2.284(10	Cd(1)-O(1)	2.351(9)
Cd(1)-O(3)	2.363(10)	Cd(1)-O(2)	2.453(9)
Cd(2)-O(8)	2.224(10)	Cd(2)-O(6)	2.250(10)
Cd(2)-O(1)#1	2.312(11)		

		1	
O(1)-Cd(1)-O(4)	142.0(4)	O(1)-Cd(1)-O(5)	106.2(4)
O(2)-Zn(1)-O(7)	155.5(4)	O(5)-Cd(1)-O(7)	97.2(5)
O(8)-Cd(2)-O(9)	93.0(6)	O(8)-Cd(2)-O(11)	174.6(6)
O(6)-Cd(2)-O(10)	173.9(5)	O(2)-Cd(2)-O(8)	88.0(4)
		O(7)#3-Zn(1)-O(11)	176.8(6)
		O(6)#5-Zn(2)-O(8)	103.4(5)

symmetry codes: #1 = -x, -y, z.

Table S3 Comparison of the selected materials in detective sensitivity for Fe^{3+} ions

Material	Sensitivity	Reference
$Eu(acac)_3@Zn(L2)_2$ (L2 =ditopic pyridyl)	5×10^{-3} M	1
$\{[H_2N(CH_3)_2]Eu(H_4L)(H_2O)\}$ (H_4L= tetrakis[4-(carboxyphenyl) oxamethyl]methane acid	2×10^{-4} M	2
$Eu(L)_3$ (L= 4′-(4-carboxyphenyl)-2,2′: 6′,2″-terpyridine)	10^{-4} M	3
$[Eu(BTPCA)(H_2O)]\cdot2DMF\cdot3H_2O$ (H_3BTPCA = 1,1′,1″-(benzene-1,3,5-triyl)tripiperidine-4-carboxylic acid	10^{-5} M	4
[Al(OH)(BDC).xsovl] (H_2BDC= 1,4-benzenedicarboxylic acid)	0.9×10^{-6} M	5
$\{[LnCd_2(DTPA)_2(H_2O)_4]\cdot4H_2O$	1.5×10^{-5} M	6
carbon nanoparticles (CNPs)	0.32×10^{-6} M	7
Fluorescent Gold Nanoclusters	5.4×10^{-6} M	8
$[Cd_3(dpa)(DMF)_2(H_2O)_3]\cdot DMF$	1.75×10^{-4} M	9
$Zn_3L_3(DMF)_2$	10^{-5} M	10
$[[Eu_2(MFDA)_2(HCOO)_2(H_2O)_6]\cdot H_2O$	1.0×10^{-4} M	11
$[Tb_4(OH)_4(DSOA)_2(H_2O)_8]\cdot(H_2O)_8$	10^{-6} M	12
1	2.2×10^{-5} M	*In this work*

[1] G. G. Hou, Y. Liu, Q. K. Liu, J. P. Ma and Y. B. Dong, *Chem. Commun.*2011, ***47***, 10731-10733.

[2] S. Dang, E. Ma, Z.M. Sun and H. J. Zhang, *J. Mater. Chem.* 2012, ***22***, 16920-16926.

[3] M. Zheng, H. Q. Tan, Z. G. Xie, L. G. Zhang, X. B. Jing and Z. C. Sun, *ACS Appl. Mater. Interfaces,* 2013, ***5***, 1078-1083.

[4] Q. Tang, S. X. Liu, Y. W. Liu, J. Miao, S. J. Li, L. Zhang, Z. Shi and Z. P. Zheng, *Inorg. Chem.*2013, ***52***, 2799-2801.

[5] C. X. Yang, H. B. Ren and X. P. Yan, *Anal. Chem.*2013, ***85***, 7441-7446.

[6] Q. Liu, F. Wan, L. X. Qiu, Y. Q. Sun and Y. P. Chen, *RSC Adv*., 2014, ***4***, 27013-27021.

[7] K. G. Qu, J. S. Wang, J. S. Ren and X. G. Qu, *Chem. Eur. J.* 2013, ***19***, 7243-7249.

[8] J.-A. A. Ho, H.-C. Chang and W.-T. Su, *Anal. Chem*. 2012, ***84***, 3246-3253.

[9] J. C. Jin, L. Y. Pang, G. P. Yang, L. Hou and Y. Y. Wang, *Dalton Trans*., 2015, ***44***, 17222–17228.

[10] Z. C. Yu, F. Q. Wang, X. Y. Lin, C. M. Wang, Y. Y. Fu, X. J. Wang, Y. N. Zhao and G. D. Li, *J. Solid. State. Chem*., 2015, ***232***, 96-101.

[11] X. H. Zhou, L. Li, H. H. Li, T. Yang and W. Huang, *Dalton Trans*., 2013, **42**, 12403–12409.

[12] X. Y. Dong, R. Wang, J. Z. Wang, S. Q. Zang and T. C. W. Mak, *J. Mater.*

Chem. A, 2015, ***3***, 641–647.

Selective adsorption behavior for dyes

Typically, 30 mg of adsorbent sample was immersed in 20 mL of aqueous dye solution containing 5×10^{-5} mol L^{-1} of dye at room temperature; the adsorption system was continually stirred.

Parameter meaning

Q_{eq} (mg g^{-1}) is the amount of adsorbed MB by **1**, C_0 (mg L^{-1}) is the initial concentration of MB in the water, and C_{eq} (mg L^{-1}) is the final concentration of MB remaining in the water. V (L) is the volume of MB solution and m (g) is the weight of **1** in this adsorption experiment.

where q_e and q_t (mg g^{-1}) are the amounts of dye adsorbed at equilibrium and t (time), respectively, and K_1 (min^{-1}) is the rate constant.

where K_2 (g mg^{-1} min^{-1}) is the pseudo-second-order rate constant.

where K_3 (g mg^{-1} min^{-1}) is the second-order rate constant.

where K_4 (mg g^{-1} $min^{-1/2}$) is the intraparticle diffusion rate constant and *C* is the boundary layer thickness.